Finite Element and Fluid-Structure Interaction Modelling of a Balloon Catheter

Junke Yao *Student Member, IEEE*, Jacob Salmonsmith, Giorgia Maria Bosi, Gaetano Burriesci, Helge Wurdemann *Member, IEEE*

***Abstract*—Intervention treatments for aortic stenosis strongly rely on the use of a medical balloon catheter which is utilized for dilating the narrowed aortic valve or the deployment of the implanted devices. However, the complete inflation of the balloon will block the blood outflow and cause instability. This paper demonstrates a computational analysis method to examine the influence of the amount of balloon inflation volume on balloon movement within a pulsating fluid environment. A tri-folded typical shape of the balloon model was inflated by pressurization. The balloon's front projection area changes during both simulation and experiment were recorded. To address the interaction between the balloon model with varying inflation levels and the introduction of fluid into the arched aorta, a Fluid-Structure Interaction (FSI) model was developed. Compared with the experimental data, the front projection area in the simulation showed a similar increment, which can be used to validate the balloon model. For FSI simulation, the balloon catheter's maximum displacement rises with the inflation level, with a slight rise at about 10 ml and a substantial rise at 20 ml volume. This work showed a significant advancement in the ability to replicate balloon movement during valvuloplasty using an FSI model.**

***Index Terms*—Valvuloplasty Balloon Catheters, Fluid-Structure Interaction, Finite Element Analysis**

I. Introduction

VALVULOPLASTY balloon catheters are a type of medical intervention devices for minimal invasive surgeries, such as transcatheter aortic valve implantation (TAVI) and balloon aortic valvuloplasty (BAV). These two intervention treatments are used to treat aortic stenosis (AS), a common heart valve disease characterised by abnormal hardening of the aortic valve leaflets that reduces the area of the valve orifice region and increases systolic ventricular pressure, typically brought on by age-related progressive calcification [1]. TAVI, introduced in 2002 to implant a prosthetic valve taking over the function of the natural valve [2], has been hailed as the preferred method for treating severe AS in patients with a medium to high risk and BAV has been usually regarded as a bridge treatment to TAVI [3]. These procedures strongly rely on using balloon catheters for valve deployment and leaflets dilatation. Current standard balloon valvuloplasty catheters have a cylindrical central action portion with two tapering ends. The complete inflation of the balloon obstructs the blood outflow tract, leading to extremely high blood pressure that can cause instability of the balloon. Rapid ventricular pacing (RVP) is employed to temporarily reduce left ventricular output for the balloon stabilization. Although it is commonly used, RVP is linked to several potential complications, including cardiac perforation, tamponade, and various arrhythmias, such as ventricular tachycardia [4]. Recent studies have focused on upgrading the device by creating non-occlusive small balloons or multi-compartment balloons in order to lessen this impact caused by the balloon catheter's characteristics [5]–[7]. However, the central orifice of these balloon catheters would unavoidably cause significant changes to the physiological flow and energy losses due to incomplete dilatation and significant aortic regurgitation. Ensuring the stability of the balloon requires to explore alternative options that can be implemented with commonly used and readily available balloon catheters.

Finite element analysis (FEA) has been shown to be a useful and practical technique for investigating and simulating the mechanical behaviours of medical devices such as folded balloons for stent expansion to examine various topics during simulations of the TAVI technique [8], [9]. However, the balloon is thought to be a secondary emphasis in the simulation of stent formation at this time, with the bulk of finite element simulation concentrating on the mechanism and behavior of stents [10]. Additionally, it is becoming increasingly important to demonstrate a numerical model's reliability, and in several recent works, experimental validations have been used to evaluate the model's ability to accurately describe the problems under study [11]–[13]. Currently, hardly a study has been done on the relationship between blood flow and the balloon catheter or standalone balloon catheter expansion modeling with experimental validation.

To investigate this concern, in this work, computer modeling methodologies are used as a starting point to examine the amount of balloon internal volume that permits its stabilization during cardiac systole. In addition, the balloon structure model is verified by comparing the information obtained from experimental testing and numerical simulations. A specific focus is put on the level of balloon inflation in order to accomplish self-stabilization during cardiac systole, considering the inflation and deflation procedures of the balloon catheter.

II. Material and Methods

The computational model of a balloon catheter with its experimental validation is built based on a specific device: Edwards 9360BC23 balloon catheter (Edwards Lifesciences, Irvine, CA, USA). The model was built and reconstructed

Junke Yao, Jacob Salmonsmith, Giorgia Maria Bosi, Gaetano Burriesci, and Helge Wurdemann are with the Department of Mechanical Engineering, University College London, UK (e-mail: junke.yao.19@ucl.ac.uk).

Gaetano Burriesci is the Group Leader of Bioengineering at Ri.MED Foundation, Palermo, Italy (e-mail: g.burriesci@ucl.ac.uk).

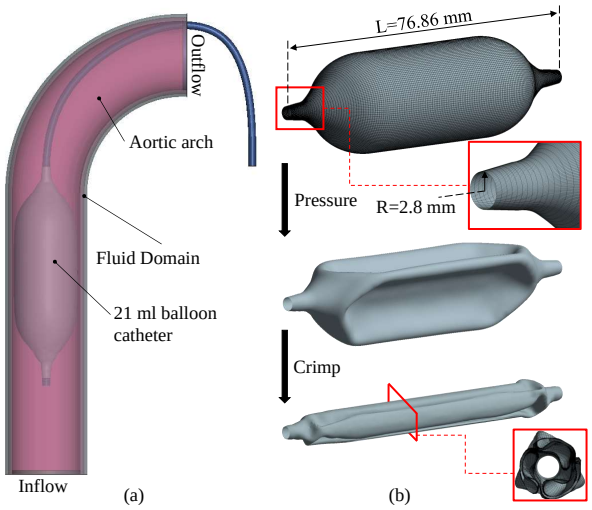

Fig. 1. (a) The numerical models of a balloon within the arched aorta immersed inside a fluid domain; (b) The finite element model of the balloon and the procedure of deflating and crimping to a tri-folded configuration.

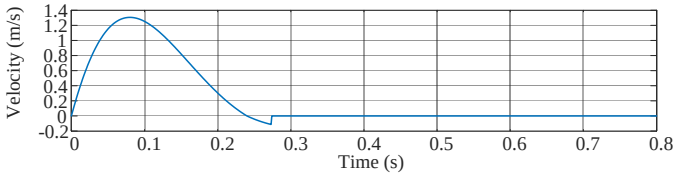

Fig. 2. The flow rate profile of the fluid when a balloon with a different inflation level is shown.

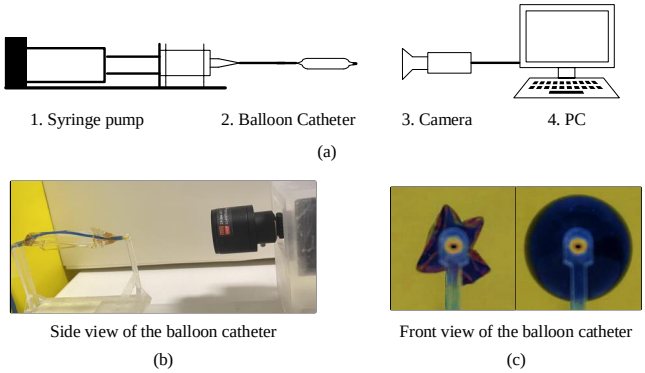

Fig. 3. (a) Illustration of the experimental setup for monitoring the balloon catheter free-inflation using a visual camera. (b) Side view of the balloon catheter and camera. (c) Front view of the balloon catheter inflated with 4 ml (left) and 21 ml (right) solution.

from an unstretched inflated balloon and then processed to a tri-folded deflated configuration for the balloon deployment simulation. The different inflated balloon models were positioned inside an idealized aortic arch with a pulsating fluid environment to investigate the relationship between the inflation level and the displacement of the balloon via FSI simulation. The experimental study was defined to obtain the device performance for the validation of the balloon catheter computational model by comparing the numerical results with the experimental outputs.

A. Numerical modeling and simulations

1) Finite Element Models: The balloon catheter model was built as a balloon with 20.75 mm diameter in an unstretched state over a bend catheter shaft with 2.8 mm diameter [14]. The action portion of the balloon is a cylindrical tube 32.8 mm long at the center, with a total length of 79.6 mm. The bend catheter is touching the wall of the aortic arch as shown in Figure 1(a), to mimic the clinical scenario. Only the systolic phase was the focus of this study, when the ventricular pressure and the ascending aorta pressure were equal, therefore, the balloon catheter was inserted in the arched aorta without considering the aortic valve. The aorta wall was modeled as a rigid body submerged in a fluid domain. The balloon's material was modelled as isotropic linear-elastic (density: 1256 $\mathrm{kg/m^3}$, Young's modulus: 600 MPa, Poisson ratio: 0.45) [15]. The catheter shaft is with a density of 1100 $\mathrm{kg/m^3}$ (Young's modulus: 1 GPa and Poisson ratio: 0.4) [16]. The fluid domain is treated as a Newtonian incompressible fluid with a density of 1060 $\mathrm{kg/m^3}$ and a dynamic viscosity of 0.004 $\mathrm{Pa \cdot s}$ [17]. In order to shorten the simulation time, the bulk modulus of fluid was assigned as 1% of the real value without affecting the analysis results [17]. The discretization of the structural model and fluid domain was performed through HyperMesh 2019 (Altair Engineering Inc., Troy, Michigan, USA). The balloon mesh consisted of 24,600 quadrilateral shell elements with 0.3 mm thickness. The shaft was discretized into 2,362 quadrilateral shell elements. The maximum stress and displacement variations with a finer mesh were decreased to less than 1%, according to a mesh sensitivity analysis, and 150 circumferential elements were sufficient to capture the balloon behaviour. The immersed-boundary method was used for solving the FSI model. The mesh of the arched aortic wall consisted of 14,560 hexahedral solid elements within a mesh of 85,760 hexahedral Arbitrary Lagrangian-Eulerian elements as the fluid domain. The elements allocated on the inlet/outlet layer were assigned as ambient at the outflow and inflow sections.

Ansys 19.0 was used for FEA simulations (ANSYS Inc., Canonsburg, USA). The commercial explicit FE solver LS-DYNA 971 (LSTC, Livermore, USA) was used to execute FSI simulations. The simulations were run on an Intel CORE i9-10900K CPU running at 3.7GHz with 64GB of RAM (Intel Corporation, Santa Clara, USA).

2) Simulation 1 - Balloon unfolding: The tri-folded deflated balloon model was created by pre-simulation via two distinct steps: a suction pressure (linearly increasing to 0.1 MPa) was applied to form a three-wings shape and an iris mechanism (12 rigid planes moved inwards) was utilized to crimp the balloon model into a tri-folded configuration (9 mm diameter), as shown in Figure 1(b). Then the unfolding/inflation procedure of the balloon was simulated by applying pressure to the inner balloon membrane until the balloon reached the nominal volume (21 ml) with two extremities fixed in all directions. To calculate their internal volume, the deformed geometry models were exported. In order to balance computational efficiency and convergence difficulty during the unfolding of the balloon,

0.8 seconds of simulation time was divided into 4 steps. For 0.2 to 0.4 seconds, when the unfolding wings and indent were expanding to a cylindrical surface, the minimum time step was set to 20 μs (otherwise, time step 2000 μs) to avoid failing to converge with large deformation.

3) Simulation 2 - Fluid-Structure Interaction: The different inflation level balloon models in unloaded status were imported into an FSI model (9 models with a 2 ml increment from 4 to 20 ml and a 21 ml). An idealised velocity waveform with a parabolic spatial profile was applied as the inlet boundary condition. This reaches a maximum value of the mean velocity equal to 1.3 m/s at the systolic peak as shown in Figure 2 [18], [19]. The peak velocity (m/s) is governed by Equation 1, where V_{in} is the velocity at the central point of the inlet surface changing with time.

$$V_{in} = \begin{cases} 2.8e^{-7.6t} sin(13.1t) & 0 \leq t \leq 0.24s \\ -0.3e^{-7.6t+1.8} sin(13.1t - 3.1) & 0.24s < t \leq 0.274s \\ 0 & 0.274s < t \leq 0.8s \end{cases} \quad (1)$$

The outlet boundary condition was zero pressure. The fluid flow was considered as laminar, and the maximum at the inlet, Reynolds number for the highest flow velocity was equal to 723. The catheter was fixed at its proximal end, allowing the bending of the catheter shaft and the displacement of balloon under the fluid action. The movements of the different balloon models along the aorta wall were calculated.

B. Experimental study

1) The balloon catheter inflation: To validate the computational models of the balloon catheter during the inflation process, the free-inflation of the balloon catheter was performed with camera recording to obtain the curve of the cross-section area and the volume inside the balloon. The setup comprised (Figure 3): an Edwards 9360BC23 balloon catheter; an automated balloon inflation device consisting of a 50 ml gas-tight syringe (ILS, Stuetzerbach, Germany) with its pump pushed by a Thomson ball screw linear actuator (PC25LX999B03-0100FM, Thomson, Kristianstad, Swede) and a Kollmorgen servo motor (Altra Industrial Motion, Braintree, MA, USA) coupling the actuator for controlling; a high-resolution camera (KAYETON 2.8-12mm varifocal USB camera); a pressure transducer (Omega Engineering Inc., Stamford, CT, USA) and a Kollmorgen AKD drive controlling the system and optimizing the performance by AKD Workbench on a PC. The camera was placed in front of the balloon to record the front-projecting view of the balloon inflation regarded as the cross-section of the balloon. Figure 3 (b) shows a side view of how the camera is placed in front of the balloon catheter. To avoid exceeding the burst pressure of the balloon, the pressure transducer was utilized to measure its real-time internal pressure.

The syringe was filled with a dark brown ink-dyed saline solution to inflate the balloon, and a bright yellow board was used as the video's background, which aided the extraction of the balloon contour during frame processing. The minimum volume of the balloon model in the FSI simulation was 4 ml, therefore the balloon was inflated to 4 ml initially; then, the

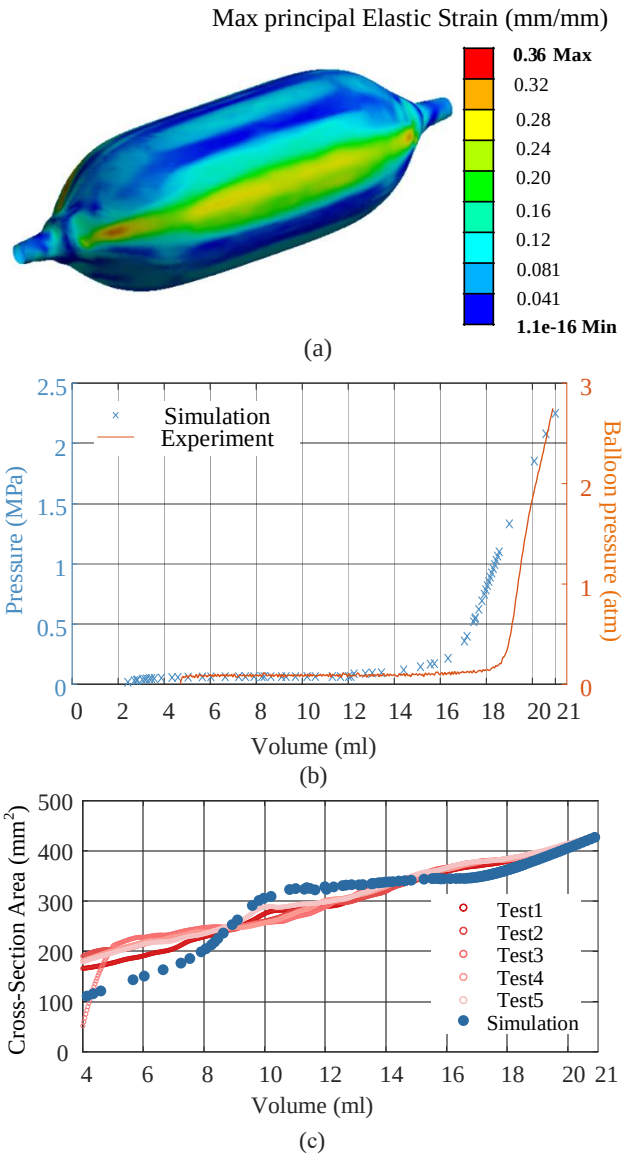

Fig. 4. The free-inflation results of the balloon catheter model. (a) The distribution of maximum principal elastic strain after pressurization. (b) The pressure-volume curve for the balloon free-inflation in simulation and experiment, where the balloon pressure is the internal pressure subtracted 1 atm. (c) The data of balloon front projection area changing with the increment of the balloon injected volume.

camera started to record the balloon front-projection view until filled to 21 ml (injection speed: 1 ml/s). Figure 3 (c) shows a front view of the catheter when filled with 4 and 21 ml. Five tests were performed and the acquired volume data and recorded videos were imported into Pycharm (JetBrains s.r.o., Praha, Czech Republic) and processed by the video processing algorithm.

2) Video processing: To analyze the results of balloon catheter free-inflation, the recorded videos were first synchronized to the obtained volume data. Then, the total pixels of the balloon representation on frames corresponding to specified volume values were extracted using the OpenCV library [20] in PyCharm. A background removal method, applying a mask

to each frame, was utilized to subtract the balloon image, and then its number of pixels was counted to calculate the area. The actual total inflated balloon diameter was 23.4 mm by measurement, resulting in the front projecting area of around 430 mm^2. Therefore, the frame containing the maximum pixel number corresponded to the balloon fully inflated with the area of 430 mm^2, which gave the real size of one pixel. The area of each frame was calculated, and the area-volume curve for each test was obtained.

III. Results

A. Balloon free-expansion

The FEA of the balloon's free-inflation took 3.5 hours to complete. Throughout the simulation, the kinetic energy to internal energy ratio remained below 5%, ensuring that internal forces were insignificant and no artificial dynamic impact arose. The three folded wings unfolded gradually within the first 0.2 s and then the balloon was almost totally unfolded within 0.01 s when the applied pressure increased to 0.05 MPa. The diameter reached about 23.4 mm at the end time. During the free-inflation, the folding edges and indent extended more than other areas, as shown in Figure 4(a). The balloon free-expansion curve is plotted in Figure 4(b), where the experimental internal pressure shows an observable increase in pressure from about 18 ml inflation and the simulation from about 16 ml inflation, with the two curves encountering at about 21 ml inflation. In particular, once the volume was increased to 10 ml, the experiments and simulation revealed agreement on the area-volume curves (Figure 4(c)). The five circle plots represent the front projecting area change with the injection volume during five tests, where the area seems to have a jump when the volume reaches 10 ml. In the simulation results, the area has a significant increase when the volume increases from 8 to 10 ml, which is followed by a flat rise until 16 ml.

B. Balloon displacements

There are ten different simulations of inflation-level balloon models. Figure 5(a) depicts the flow rate distribution around the balloon at 0.13 seconds. As the injected volume increases from 8 to 10 ml, the local flow velocity between the balloon and the inner wall of the aorta increases. The maximum displacement of the balloon models along the aorta versus volume are displayed in Figure 5(b), with values of 1.22, 1.48, and 1.81 mm for 4 to 8 ml and a jump from 8 to 10 ml (3.24 mm). The maximum displacement increases from 3.76 to 5.08 mm at injected volume ranging from 12 to 18 ml. The maximum value climbs to 9.55 mm for the 20 ml balloon and to 18.47 mm for the 21ml balloon. The displacement of the 21 ml balloon is noticeably bigger than others. The size of the circles in Figure 5(b) at each injected volume is related to the ratio between the balloon model's cross-section area and the aorta section area: 0.17, 0.29, 0.44, 0.70, 0.71, 0.73, 0.76, 0.84, 0.94, 1.00.

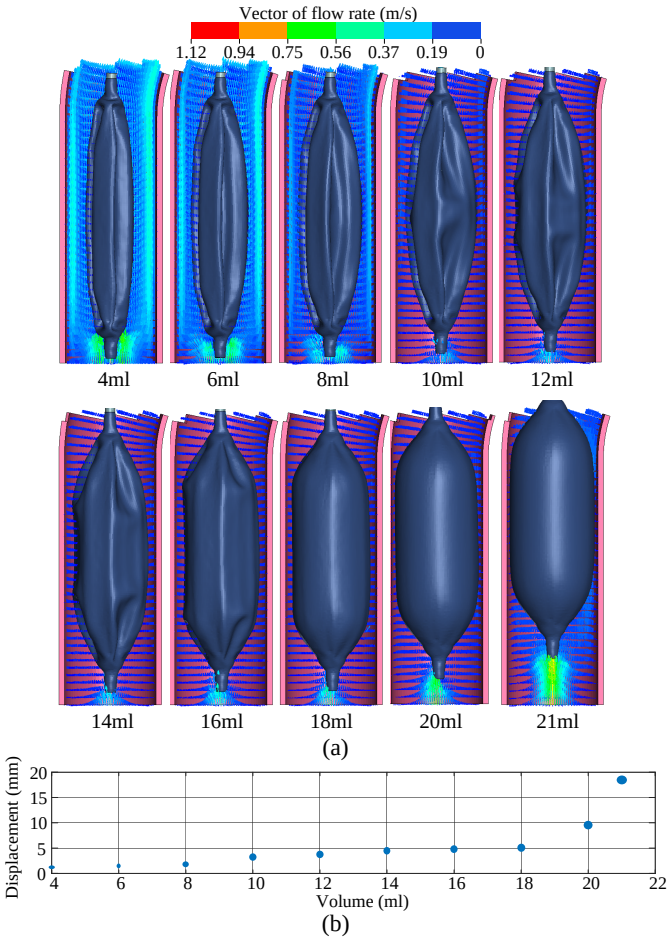

Fig. 5. (a) FSI simulation results and (b) the maximum displacement of the balloon along the aorta for each balloon model extracted from simulation.

IV. Discussion and Conclusion

The balloon catheter's form and contour changes during the inflation process were the primary focus of the balloon's FE numerical model, which enabled a comprehensive analysis of its geometry. The highest elastic strain occurred on the folded kink point when the balloon was in the tri-folded configuration. The pressure-volume curve from the simulation showed that the internal pressure of the balloon increased sharply from 16 ml, followed by a linear increment, similar to the experimental trend shown in Figure 4(b). The front projection of the balloon during free-inflation simulation shows a significant increment from 8 to 10 ml of injected volume, and followed by a relatively slow rise until 18 ml. In the experiment, the change in the front projection of the balloon shows a more linear increment with small fluctuations when the balloon is inflated until 10 ml of injected volume. Broadly speaking, the simulated and experimental curves show a similar trend of expansion and both curves reach about 430 mm^2 for an injected volume of 21 ml. Above 10 ml, the overlap between the simulation and the experimental data becomes more relevant, suggesting that balloon models at different inflation levels can be confidently used in the simulation based on the balloon contour influence. Comparison between the experimental and computational shapes taken by the balloon during inflation

needs to take into account that the numerical model achieves inflation by direct application of a transmural pressure and does not capture the fluid dynamics that participates in the process in the physical balloon. This necessarily implies some difference in the cross-sectional geometries. However, this variation does not result in a significant difference in the cross-sectional area, which has the largest influence on the subsequent FSI simulation.

Different levels of balloon inflation within the pulsating fluid environment were simulated by FSI simulations. The sharp increases observed in balloon displacement (when the volume changes from 8 to 10 ml and from 18 to 20 ml) show that there is a volume threshold over which the balloon can produce noticeable displacement and another one at which the displacement of the balloon will climb quickly (see Figure 5(b)). These sudden jumps were also reflected in the free-inflation simulation of the balloon, where the front projection area showed a higher slope between 8 to 10 ml and after 18 ml than at other inflation levels. Given that the displacement, in this case, below a volume of 10 ml, is only a modest amount (<2 mm for balloon moving distance along the aorta under the systolic blood flow), it may be inferred that the balloon is comparatively stable. By frequently deflating the balloon to a "safe volume" (i.e., 10 ml) during systole and repeatedly inflating it to the nominal capacity to induce valve expansion during diastole until effective dilatation, stability can be achieved while avoiding the issues connected to heart pacing. These results offer a potential explanation of how to pace balloon inflation rather than the left ventricular during valvuloplasty to avoid heart pacing.

In the future, considering the material anisotropy of the aortic wall and incorporating the aortic sinuses and leaflets to represent a more realistic anatomical configuration will allow the simulation to provide more accurate results. In addition, an experimental study for FSI model validation will be carried out by connecting the simulation phantom to a pulse duplicator.

REFERENCES

[1] K. Amrit, J. T. Jeremy, and V. T. Nkomo, "Management of patients with aortic valve stenosis," *Mayo Clinic Proceedings*, vol. 93, no. 4, pp. 488–508, 2018.

[2] A. Cribier, H. Eltchaninoff, A. Bash, N. Borenstein, C. Tron, F. Bauer, G. Derumeaux, F. Anselme, F. Laborde, and M. B. Leon, "Percutaneous Transcatheter Implantation of an Aortic Valve Prosthesis for Calcific Aortic Stenosis," *Circulation*, vol. 106, no. 24, pp. 3006–3008, 2002.

[3] T. R. Keeble, A. Khokhar, M. M. Akhtar, A. Mathur, R. Weerackody, and S. Kennon, "Percutaneous balloon aortic valvuloplasty in the era of transcatheter aortic valve implantation: a narrative review," *Open Heart*, vol. 3, no. 2, p. e000421, 2016.

[4] B. M. Jones, Y. Jobanputra, A. Krishnaswamy, S. Mick, M. Bhargava, B. L. Wilkoff, and S. R. Kapadia, "Rapid ventricular pacing during transcatheter valve procedures using an internal device and programmer: A demonstration of feasibility," *Catheterization and Cardiovascular Interventions*, vol. 95, no. 5, pp. 1042–1048, 2020.

[5] A. Shivaraju, C. Thilo, N. Sawlani, I. Ott, H. Schunkert, W. Von Scheidt, A. Kastrati, and A. M. Kasel, "Aortic Valve Predilatation with a Small Balloon, without Rapid Pacing, prior to Transfemoral Transcatheter Aortic Valve Replacement," *BioMed Research International*, vol. 2018, no. February 2014, pp. 2–7, 2018.

[6] S. Toggweiler, L. Loretz, M. Brinkert, M. Bossard, M. Wolfrum, F. Moccetti, B. Berte, F. Cuculi, and R. Kobza, "Simplifying transfemoral accurate neo implantation using the trueflow nonocclusive balloon catheter," *Catheterization and Cardiovascular Interventions*, vol. 96, no. 6, pp. E640–E645, 2020.

[7] R. Hofmeyr, J. McGuire, K. Park, M. Proxenos, S. Peer, M. Lehmann, and D. Lubbe, "Prospective observational trial of a nonocclusive dilatation balloon in the management of tracheal stenosis," *Journal of Cardiothoracic and Vascular Anesthesia*, 2022.

[8] M. Bianchi, G. Marom, R. P. Ghosh, H. A. Fernandez, J. R. Taylor, M. J. Slepian, and D. Bluestein, "Effect of Balloon-Expandable Transcatheter Aortic Valve Replacement Positioning: A Patient-Specific Numerical Model," *Artificial Organs*, vol. 40, no. 12, pp. E292–E304, 2016.

[9] G. M. Bosi, C. Capelli, M. H. Cheang, N. Delahunty, M. Mullen, A. M. Taylor, and S. Schievano, "Population-specific material properties of the implantation site for transcatheter aortic valve replacement finite element simulations," *Journal of Biomechanics*, vol. 71, pp. 236–244, 2018.

[10] S. Morlacchi and F. Migliavacca, "Modeling Stented Coronary Arteries: Where We are, Where to Go," *Annals of Biomedical Engineering*, vol. 41, no. 7, pp. 1428–1444, 2013.

[11] T. Qiu and L. Zhao, "Research into biodegradable polymeric stents: A review of experimental and modelling work," *Vessel Plus*, vol. 2, p. 12, 2018.

[12] M. A. Geith, K. Swidergal, B. Hochholdinger, T. G. Schratzenstaller, M. Wagner, and G. A. Holzapfel, "On the importance of modeling balloon folding, pleating, and stent crimping: An FE study comparing experimental inflation tests," *International Journal for Numerical Methods in Biomedical Engineering*, vol. 35, no. 11, pp. 1–19, 2019.

[13] L. Wiesent, U. Schultheiß, C. Schmid, T. Schratzenstaller, and A. Nonn, "Experimentally validated simulation of coronary stents considering different dogboning ratios and asymmetric stent positioning," *PloS one*, vol. 14, no. 10, p. e0224026, 2019.

[14] B. Benedetta, L. Giorgia, M Bosiand Valentina, J. Rod, T. Spyros, B. Gaetano, M. Francesco, M. T. Andrew, S. Silvia, and B. Giovanni, "Numerical model of a valvuloplasty balloon: in vitro validation in a rapid-prototyped phantom." *BioMed Eng OnLine*, vol. 15, no. 37, pp. 1–6, 2016.

[15] F. Sturla, M. Ronzoni, M. Vitali, A. Dimasi, R. Vismara, G. Preston-Maher, G. Burriesci, E. Votta, and A. Redaelli, "Impact of different aortic valve calcification patterns on the outcome of transcatheter aortic valve implantation: A finite element study," *Journal of Biomechanics*, vol. 49, no. 12, pp. 2520–2530, 2016.

[16] D. Martin and F. Boyle, "Sequential Structural and Fluid Dynamics Analysis of Balloon-Expandable Coronary Stents: A Multivariable Statistical Analysis," *Cardiovascular Engineering and Technology*, vol. 6, no. 3, pp. 314–328, 2015.

[17] F. Sturla, E. Votta, M. Stevanella, C. A. Conti, and A. Redaelli, "Impact of modeling fluid–structure interaction in the computational analysis of aortic root biomechanics," *Medical Engineering and Physics*, vol. 35, no. 12, pp. 1721–1730, 2013.

[18] K. Cao and P. Sucosky, "Effect of bicuspid aortic valve cusp fusion on aorta wall shear stress: Preliminary computational assessment and implication for aortic dilation," *World Journal of Cardiovascular Diseases*, vol. 5, pp. 129–140, 05 2015.

[19] O. Smadi, I. Hassan, P. Pibarot, and L. Kadem, "Numerical and experimental investigations of pulsatile blood flow pattern through a dysfunctional mechanical heart valve," *Journal of Biomechanics*, vol. 43, no. 8, pp. 1565–1572, 2010.

[20] G. Bradski, "The OpenCV Library," *Dr. Dobb's Journal of Software Tools*, 2000.